OBSERVATIONS OF DYNAMIC STALL PHENOMENA ON AN OSCILLATING AIRFOIL WITH SHEAR-STRESS-SENSITIVE LIQUID CRYSTAL COATINGS

Daniel C. Reda*
Sandia National Laboratories
Albuquerque, NM 87185
U.S.A.

ABSTRACT

Oscillating airfoil experiments were conducted using shear-stress-sensitive/temperature-insensitive liquid crystal coatings in order to investigate unsteady fluid physics associated with the dynamic-stall process. Laser-light-sheet/smoke-particle flow visualization and surface-mounted micro-tufts were also employed to complement the liquid crystal technique. A color video camera was used to record all observations. Experiments were conducted under incompressible flow conditions at a freestream Reynolds number (based on chord) of ~ 10^6. Angle-of-attack oscillations of ± 19° about 0°, at several discrete frequencies, were used to induce the unsteady flows. Boundary layer transition and turbulent separation locations were seen to undergo extensive and rapid movements with changing angle of attack, particularly on the airfoil lee surface. Progression of turbulent separation to the immediate vicinity of the leading edge was observed to result in large-scale, three-dimensional fluctuations in the surface shear stress pattern. Frame-by-frame analyses of the video record indicated this phenomenon to be a result of a quasi-periodic (~ 2 hertz) "switching" of the flow between attached and separated states over large portions of the airfoil lee surface. Comparisons of transition and turbulent separation measurements with Eppler code predictions indicated that the empirically-based viscous flow modeling used in this design tool requires updates.

NOMENCLATURE

C chord length

C_L lift coefficient = $\dfrac{F_L}{\frac{1}{2}\rho_\infty U_\infty^2 C}$

f frequency of oscillation

f_s flow "switching" or "shedding" frequency

F_L lift force per unit span

k reduced frequency = $\dfrac{\pi f C}{U_\infty}$

t time

u' freestream velocity fluctuations

U_∞ freestream velocity

X distance along chord line from leading edge

Y distance measured perpendicular to chord line

α' angle-of-attack amplitude

$\bar{\alpha}$ mean angle of attack

α instantaneous geometric angle of attack (positive denotes leeside)

ρ_∞ freestream density

INTRODUCTION

Unsteady boundary layer flows occur on airfoil surfaces of wind energy conversion systems, rotary-wing aircraft, and maneuvering fixed-wing aircraft. In such flows, the dynamic movement of boundary layer transition is of importance due to its direct influence on the unsteady surface shear stress distribution. Further, as a result of coupling between the "state" of the boundary layer (laminar versus turbulent) and boundary layer separation phenomena, transition zone movement can also strongly influence the unsteady surface pressure distribution. For transient angle-of-attack excursions beyond an airfoil's static-stall limit, complex leading-edge-separation/vortex-shedding ("dynamic stall") phenomena occur. An excellent review of the state-of-the-art concerning dynamic stall phenomenology was recently given by Carr.[1]

In the present research, newly formulated (shear-stress-sensitive/temperature-insensitive) liquid crystal coatings were applied to the surface of an oscillating airfoil in order to investigate the unsteady fluid physics associated with the dynamic stall process. Surface-mounted micro-tufts and laser-sheet/smoke-particle flow visualization were also utilized to complement the liquid crystal technique. Dynamic boundary layer transition and turbulent separation locations were measured as a function of geometric angle of attack, and results are presented in comparison with predictions generated with the Eppler airfoil design code.[2,3]

LIQUID CRYSTALS

Liquid crystals are highly anisotropic "fluids" that exist between the solid and isotropic liquid phases of some organic compounds.[4,5] As such, they exhibit optical properties characteristic of a crystalline (solid) state, while displaying mechanical properties characteristic of a liquid state.

*Senior Member Technical Staff;
Associate Fellow, AIAA

In aerodynamic flow-visualization applications, a mixture of one part liquid crystals to five to eight parts solvent (here, trichlorotrifluoroethane) is sprayed on the aerodynamic surface under study (a flat-black surface is essential for color contrast). Recommended applications (after spray losses) are ~ 10 ml liquid crystals, measured prior to mixing with the solvent, to each square meter of surface area. The solvent evaporates, leaving a uniform thin film (approximately 10^{-3} cm in thickness) which selectively scatters incident white light as discrete colors.

This behavior is traced to the molecular structure of the compounds, a helical structure whose characteristic pitch length falls within the wavelength range of the visible spectrum. For "thermochromic" liquid crystals, the two primary factors that influence this molecular structure (and thus the light-scattering response of the liquid crystal coating) are temperature and surface shear stress. In low-speed incompressible flows, wherein temperature is (or can be held) essentially constant, the shear stress dependence dominates.. Surface color patterns are then displayed in response to varying surface shear stress loads, once some threshold level of shear stress has been exceeded. So long as the chemical structure of the liquid crystals remains unaltered, temperature and/or shear stress responses are theoretically rapid and reversible indefinitely. The challenge in such aerodynamic applications is to quantify, or at least demonstrate, that the color change/frequency response of this technique is consistent with the mean and time-varying shear stress levels encountered in the flows under investigation.

The literature shows several applications of this technology to fluid mechanics research. The first was by Klein[6], who used the temperature response of liquid crystals in high-speed/compressible flows to measure surface temperature contours from which transition locations were inferred. Attempts to de-couple the influences of temperature and shear stress, and to make quantitative measurements of shear stress under isothermal flow conditions, were difficult and generally not productive[7]. A hiatus ensued, until the recent investigations by NASA-Langley researchers,[8,9,10] who successfully applied this technique as a qualitative shear stress (boundary layer transition) indicator in subsonic flight tests of airplanes.

More recently, oscillating airfoil experiments were conducted by Reda[11] to test the frequency response of thermochromic liquid crystal coatings to unsteady surface shear stresses under isothermal-flow conditions. The model was an NACA-0015 airfoil, exposed to an incompressible flow at a freestream Reynolds number (based on chord) of 10^6. Angle-of-attack forcing functions were sine waves of amplitude ± 10° about each of three mean angles of attack: 0°, 10°, and 20°. Frequencies of oscillation were 0.2, 0.6 and 1.2 hertz. Data acquisition was accomplished by video recording. Observations showed the liquid crystal technique capable of making high surface shear stress zones visible over the stated dynamic range in a continuous and reversible manner. As an extension of this work, the feasibility of applying the liquid crystal technique to field tests of operating wind turbines was also successfully demonstrated.[12,13]

Very recent advances in liquid crystal technology have led to the formulation of compounds that display no temperature response over broad temperature regimes; for these mixtures, color changes result solely in response to applied shear stress, making them potentially more suitable for aerodynamic flow-visualization applications.[14]

Additional oscillating, and post-stall static, airfoil experiments were conducted by Reda and Butterfield[15] to test the frequency response of these new shear-stress-sensitive/temperature-insensitive liquid crystal coatings. A full-span model of the SAND 0018/50 airfoil (described below) was exposed to incompressible flows at a freestream Reynolds number (based on chord) of 10^6. The angle-of-attack forcing function was a sine wave of amplitude ± 10° about a mean angle of 0°. Frequencies of oscillation were 0.2, 0.6 and 1.2 hertz, corresponding to reduced frequencies of 0.006, 0.018 and 0.037. Post-stall static experiments were conducted at a fixed angle of attack of 14°, a condition that yielded unsteady leading-edge separation phenomena. Data acquisition was accomplished by video recording. Observations of boundary layer transition zone movement and unsteady leading-edge shear stress fluctuations showed that these liquid crystal coatings are capable of making transient surface shear stress events visible over the stated dynamic range, in a continuous and reversible manner, with a color-change response time of less than 0.03 seconds (the framing rate of standard video equipment). These shear-stress-sensitive/temperature-insensitive liquid crystal coatings were thus employed in the present research to investigate dynamic-stall phenomena on the SAND 0018/50 airfoil.

One final comment concerning the use of liquid crystal coatings in fluid mechanics research is in order. As noted above, attempts to "calibrate" the shear stress-versus-color relationship of a given liquid crystal compound were undertaken by Klein and Margozzi.[7] In this technique, the "absolute" color (for a given shear stress) seen by the observer (or recording device) is a function of lighting and view angles. Therefore, transformation of any such calibration curve from the calibration apparatus to the aerodynamic test facility results in significant uncertainties, especially for complex surface contours. While "in-situ" calibration of the liquid crystal coating may be possible, one would then have to measure the distribution of shear stress acting on the test surface with some other technique (e.g., flush-mounted hot-film sensors). Calibration of these devices would also be required. Given these difficulties, no calibration of the coating's color with the magnitude of the surface shear stress imposed upon it was attempted. It is felt that the liquid crystal technique is best utilized to "visualize" the presence/location of high surface shear stress zones in time-varying flows (through observations of relative changes in surface color patterns), while measurements of surface shear stress distributions are best accomplished with arrays of calibrated/point sensors.

AIRFOIL AND TEST CONDITIONS

The airfoil employed in the present research is the SAND 0018/50 (see Figure 1 and Table 1); the "18" denotes an 18-percent (of chord) maximum thickness, while the "50" denotes a design specification for a 50-percent (of chord) run length of laminar flow at zero angle of attack. This symmetric airfoil was designed specifically for vertical axis wind turbine (VAWT) applications by G. M. Gregorek[16] of Ohio State University using the Eppler code.[2,3] Its two principal performance characteristics are:
(1) reasonable lift, coupled with low drag, at low angles of attack (for improved VAWT electrical power generation at low to intermediate wind speeds); and
(2) an abrupt-stall behavior at angles of attack near 13° (for passive or "built-in" power regulation of the VAWT at high wind speeds). Low drag at low angles of attack is achieved through contour shaping, the resultant favorable pressure gradient from leading

edge to mid-chord tending to increase boundary layer stability within this region, thereby promoting the maintenance of low-skin-friction laminar flow. Sharp-stall behavior is achieved through the incorporation of a small-radius-of-curvature leading edge (~ 0.01C). A 0.91 m (3')-span, 0.35 m (14")-chord model of this contour was fabricated for wind-tunnel testing.

Experiments were conducted at the Ohio State University 0.91 m x 1.52 m (3' x 5') open-return subsonic wind tunnel. Freestream Reynolds number, based on chord length and a freestream velocity ~ 36.5m/sec (120 ft/sec), was order 10^6. Freestream turbulence intensity (u'/U_∞) at these test conditions was measured to be 0.0015.

The model was mounted vertically, fullspan, from floor to ceiling, and was driven in angle-of-attack oscillations (about the midchord) by a variable-speed electric motor/mechanical cam and linkage system located below the test section floor. Angle-of-attack versus time histories were defined by an arc-tangent function with the following equation and parameters (see Figure 2):

$$\tan \alpha = \frac{\sin (2\pi ft)}{3.0715 + \cos (2\pi ft)} \qquad (1)$$

amplitude (α') = ± 19°

mean angle ($\bar{\alpha}$) = 0°
frequency (f) = ~ 0, 0.2, 0.6 hertz
reduced frequency (k) = ~ 0, 0.006, 0.018

The arc-tangent function was used because it defines the geometric angle-of-attack history experienced by the rotor of a VAWT at the equator height.[17,18]. The value of the constant (here, 3.0715) corresponds to the tip speed ratio of the VAWT (blade rotational speed-to-wind speed).

DATA ACQUISITION

A shear-sensitive/temperature-insensitive liquid crystal coating was applied to the airfoil surface, from leading edge to trailing edge and over a span width of order one chord length, in order to make the dynamic surface-shear-stress patterns visible. In addition, a single chord-wise line of micro-tufts (0.15 mm-diameter, ~ 25.4 mm-long, white-thread segments) was applied to the airfoil surface immediately adjacent to the liquid crystal zone in order to make the presence/location of boundary layer separation visible. The laser-light-sheet/smoke-particle flow visualization technique was also employed, in a plane perpendicular to the airfoil chord plane, to complement the surface flow visualization techniques.

Data acquisition was accomplished with a Hitachi model FPC3 video camera recording at 30 frames/second onto 3/4" tape. Polarizing filters were used on both the illumination sources and the video camera lens in order to minimize reflected glare. No-flow video records were taken for both static and oscillating angle-of-attack conditions in order to define baseline light-reflection patterns.

Geometric angle of attack was measured with an angular potentiometer attached to the drive shaft of the oscillation mechanism. Angle-of-attack values were displayed on a digital readout device and recorded on a separate video tape. Time-code signals (from a single time-code generator) were fed onto both the liquid-crystal and angle-of-attack video records, allowing for post-test superposition of the two records.

VISUAL OBSERVATIONS

A summary of the dynamic visual observations exists in the form of a 13-minute color video. Interested researchers may request a copy of this tape by writing to the author. A written description of these visual observations is given below. Quantitative measurements of transition and turbulent separation locations as functions of geometric angle of attack (as taken from the video record) will be presented in the next section in comparison with Eppler code predictions.

One difficulty experienced in documenting this research concerned the "transformation" of a dynamic color video record to still black-and-white photographs suitable for printing/reproduction. An individual color video frame, when "frozen," generally did not yield a quality black-and-white print. As a result, only two black-and-white photographs are presented in the text, but these are supported with flowfield schematics and graphical data.

Observations of liquid crystal and micro-tuft responses were first made for the case of a slowly increasing α (from 0° to +19°), prior to the oscillating - α cases at 0.2 and 0.6 Hz.

In the absence of flow (zero surface shear stress), the liquid crystal coating exhibited a uniform "rusty red" color. With the onset of steady flow at α = 0°, the color pattern changed to the following distribution (Figure 3 shows a black and white photograph): light yellow from leading edge to near mid-chord, gradually fading back to the original rusty red color at (X/C) ~ 0.5; rusty red in the region ~ 0.5 < (X/C) < ~ 0.65; bright yellow at (X/C) ~ 0.65, remaining yellow to the trailing edge. This response indicated a low-shear-stress laminar boundary layer from leading edge to mid-chord; a laminar separation bubble (induced by the contour-generated adverse pressure gradient) in the region 0.5 < (X/C) < 0.65, with transition to turbulence occurring in the separated shear layer above the reverse-flow (essentially zero-shear-stress) region; a high-shear-stress turbulent reattachment zone at (X/C) ~ 0.65, followed by a high-shear-stress (attached) turbulent boundary layer to the trailing edge (see schematic of Figure 4).

As α was slowly increased (positive α denoting leeside flows visible to the camera), the turbulent reattachment (straight/bright yellow) "line" edged forward, then, at α = 5.5°, abruptly flashed forward. This observation illustrated the disappearance (possible "bursting") of the laminar separation bubble, transition then occurring within the attached laminar boundary layer between the leading-edge and mid-chord locations. This light-yellow/dark-yellow transition "front" appeared ragged along its span-wise extent (see black and white photo of Figure 5).

At α = 8.5°, transition had progressed all the way forward to the immediate vicinity of the leading edge. Close examination of the steady-state color pattern at α = 10° indicated the re-establishment of a small laminar separation bubble at the leading edge, once again causing transition to turbulence (see schematic of Figure 6). The overall color pattern on the airfoil surface for 8.5° ≤ α < 12.5° indicated (via bright yellow shades) the existence of an attached turbulent boundary layer from just downstream of the leading-edge bubble rearward to beyond the mid-chord location, where a gradual return of the original rusty-red color was observed.

Consistent with this interpretation, the line of micro-tufts clearly showed the onset of turbulent boundary layer separation to occur at the trailing edge at $\alpha = 6.5°$, with separation progressing continuously forward to (X/C) ~ 0.5 at $\alpha = 12.5°$. At this point, a one-degree increase in α (to 13.5°) caused turbulent separation to flash to the immediate vicinity of the leading edge.

Concurrent with this rapid forward movement of turbulent separation to the leading edge, the liquid crystal coating showed the onset of unsteadiness in the surface shear stress pattern in, and downstream of, the leading-edge region. These shear-stress fluctuations occurred as large-scale, three-dimensional events and were felt to be associated with vortical structures shed from the airfoil leading edge and then convected rearward over the airfoil lee surface by the outer/inviscid flow (see schematic of Figure 7). This unsteady response was seen in the liquid crystal coating over the regime $13.5° \leq \alpha \leq 17.5°$ under both static (f = 0 Hz) and dynamic (f = 0.2 and 0.6 Hz) conditions.

To investigate this unsteady phenomenon in more detail, frame-by-frame analyses of the $\alpha = 14°$ video record were conducted. Liquid crystal and micro-tuft responses, when viewed in this manner, both clearly indicated the presence of a quasi-periodic "switching" of the flow between separated and attached states over large portions of the airfoil lee surface. Frequency of "flow switching" was measured via the liquid crystal technique to be ~ 2.2 hertz, a value well within the frequency-response range of this technique. The micro-tuft approach yielded corroborating results (at ~ 1.4 hertz), but the frequency response of this method, as applied in the present research, remains unquantified. Using hot-wire anemometry, Zaman[19] observed similar leading-edge flow unsteadiness (in the 5 to 10 hertz range) for steady flows over several different airfoils placed at, or just beyond, their respective static-stall angle of attack. Utilizing his observed mid-range frequency of ~ 7.5 hertz, Zaman converted these results into a dimensionless frequency (or Strouhal number) $[f_s C \sin \alpha]/U_\infty \sim 0.02$, a value well below the established bluff-body/vortex-shedding value of ~ 0.2. Present results yielded a value for this dimensionless frequency of ~ 0.005, in general agreement with Zaman's findings.

On the windward side ($\alpha = 0°$ to - 19°), the laminar separation bubble and high-shear-stress turbulent reattachment zone were observed to exist near mid-chord for $0° > \alpha > - 5.5°$, followed by a rearward movement of transition to (X/C) ~ 0.95 at $\alpha = - 19°$. As expected, the micro-tufts showed no turbulent boundary layer separation from the windward side of the airfoil.

Observations of transition and turbulent separation locations made using the liquid-crystal and micro-tuft techniques were found to be reversible and repeatable over the frequency-of-oscillation regime investigated here. No measurable dependence of these locations on frequency was apparent. However, independent surface pressure measurements taken on this airfoil under the same test conditions (by Gregorek[20] and Hoffmann[21]), when integrated over the airfoil surface, showed the existence of "hysterisis loops" in the lift coefficient and pitching moment coefficient versus angle-of-attack curves (e.g., see Figure 8). Despite the relatively low values of reduced frequency imposed here, unsteady loads, dependent on the frequency of oscillation, were experienced by the SAND 0018/50 airfoil, consistent with dynamic-stall events observed on other airfoils.[1]

The laser-light-sheet/smoke-particle flow visualization technique yielded results that both corroborated and supplemented the liquid-crystal and micro-tuft observations. In these experiments, a glycerin smoke generator, with a rectangular exhaust nozzle of ~ 7 cm height and ~ 38 cm span, was positioned within the wind tunnel plenum chamber. The smoke "plane" traversed a honeycomb sheet, three screens, and the contraction section before passing over (in alignment with) the airfoil leading edge at its $\alpha = 0°$ position. The laser-light plane was perpendicular to the airfoil chord plane, and the smoke pattern in this lighted plane was recorded by video camera from an essentially side-on view. Clearly, at a recording speed of 30 frames/second, this technique could only be expected to show overall features of the time-varying flow fields, not "turbulence structure." Despite this limitation, three interesting observations were noted.

First, under oscillating-α conditions, the smoke-tagged streamlines (that had passed over the airfoil leading edge at the fixed $\alpha = 0°$ condition) were consistently deflected toward the instantaneous lee (low-pressure) side of the airfoil. Second, based on observations of inviscid flow streamline deflections, the extent of airfoil upstream influence on the approaching flow was seen to be of the order of one chord length. And, third, the smoke-tagged streamlines appeared to "burst" at the airfoil leading edge simultaneously with the occurrence of turbulent boundary layer separation flashing from mid-chord to the leading edge. A large-scale unsteady vortical structure then formed above the lee surface. This vortex convected smoke from the outer-flow streamlines inward toward the lee surface, then upstream along this surface toward the leading edge. Unsteadiness ("flapping") in the outer-flow streamlines also occurred during this event.

BOUNDARY LAYER TRANSITION AND TURBULENT SEPARATION MEASUREMENTS VERSUS EPPLER CODE PREDICTIONS

The Eppler airfoil design and analysis code[2,3] incorporates a conformal-mapping approach for the design of contours with prescribed velocity distributions and a panel-method approach for computation of the potential (outer/inviscid) flow field about a specified contour at any desired constant angle of attack. The potential-flow pressure distribution around an airfoil surface, at any fixed angle of attack, can thus be obtained. The boundary layer (inner/viscous) flow that develops within the prescribed potential-flow pressure distribution is calculated using integral techniques applied to the momentum and energy equations. These viscous-flow computations rely heavily on empirically-defined inputs. For example, both laminar and turbulent boundary layer separation are predicted based on the attainment of some critical shape factor (ratio of energy thickness to momentum thickness) defined, in each case, by empirical values. Transition from laminar to turbulent flow is likewise defined by an empirical correlation based on computed integral length scales. The outer/inviscid flow is not corrected (iterated upon) to account for either boundary layer displacement or boundary layer separation effects. Predicted forces and moments on the airfoil surface are, therefore, expected to become less accurate as the predicted extent of separated flow increases.[22] Such conditions are encountered at angles of attack well below the static-stall (leading-edge-separation) limit (here, $\alpha = 13.5°$).

Given the fact that the modeling of the viscous flow physics within this design code is strongly dependent on previous experimental observations (for specific

airfoil contours), it is desirable to test the validity of this modeling for other (newly-designed) airfoil contours.

Frame-by-frame analyses of the video records (described in the previous section) allowed boundary layer transition and turbulent separation locations to be measured on the SAND 0018/50 contour as functions of geometric angle of attack. Figure 9 shows measured results in comparison with Eppler code predictions. Transition and turbulent separation locations, measured on both the windward and leeward surfaces, were found to exhibit the same general trends with variations in angle of attack as predicted by the Eppler code. However, quantitative differences were noted.

First, concerning transition to turbulence, surface shear stress patterns made visible by the liquid crystal technique clearly showed the existence of a laminar separation bubble beginning just downstream of the mid-chord position for $-5.5° \leq \alpha \leq +5.5°$, with a high shear stress turbulent reattachment zone occurring immediately downstream of the reverse-flow region. This experimental observation was also seen during liquid-crystal field tests conducted on the same airfoil contour at low angles of attack.[12] For $|\alpha| < 5.5°$, transition to turbulence thus occurred in the separated shear layer above the bubble, not in an attached laminar boundary layer. (Note: The Eppler code predicted transition to result from, and to be coincident with, laminar separation for $\alpha \leq 4°$ on the leeside; details of the laminar separation bubble are not computed in this code.) Even with allowances for the fact that measured "transition" locations for $-5.5° \leq \alpha \leq +5.5°$ were actually turbulent reattachment locations, data taken over the complete angle-of-attack regime ($-19° \leq \alpha \leq +19°$) showed the Eppler code to be conservative in its transition prediction capabilities, i.e., predicted transition locations were consistently upstream of measured locations.

Measured locations for turbulent boundary layer separation were also found to be in quantitative disagreement with predicted values. Onset of the forward progression of turbulent separation from the trailing edge occurred at $\alpha = 6.5°$, as compared to the predicted incipient separation angle of attack of 4°. Both the rate of forward progression and the forward-most quasi-stable location for turbulent separation were observed to be in disagreement with Eppler code predictions. Finally, turbulent separation was observed to flash to the immediate vicinity of the leading edge for $\alpha \sim 12.5°$, as compared to a predicted static-stall angle of 11°.

SUMMARY

1. Surface shear stress visualization with liquid crystal coatings provides a powerful diagnostic technique for investigations of unsteady viscous flows.

2. Boundary layer transition and turbulent separation locations can experience extensive and rapid movements over airfoil surfaces undergoing angle-of-attack changes (particularly on lee surfaces).

3. Progression of turbulent separation to the immediate vicinity of the airfoil leading edge was seen (via the liquid crystal technique) to result in large-scale, three-dimensional fluctuations in the surface shear stress distribution. Frame-by-frame analyses of the video record indicated this unsteady phenomenon to be a result of a quasi-periodic (~ 2 hertz) "switching" of the flow between attached and separated states over large portions of the airfoil lee surface.

4. Comparisons of present results with predictions generated via the Eppler airfoil-design code indicate that the (empirically-based) viscous flow modeling within this code requires improvements.

ACKNOWLEDGMENTS

This research was sponsored by the U.S. Department of Energy, Wind/Ocean Technologies Division, under contract DE-AC04-76DP00789.

The assistance of G. M. Gregorek and M. J. Hoffmann, Aeronautical and Astronautical Research Laboratory, Ohio State University, is gratefully acknowledged.

REFERENCES

1. Carr, L. W., 1988, "Progress in Analysis and Prediction of Dynamic Stall," AIAA J. Aircraft, V25, pp. 6-17.

2. Eppler, R. and Somers, D. M., 1980, "A Computer Program for the Design and Analysis of Low-Speed Airfoils," NASA Tech. Memos 80210 and 81862.

3. Eppler, R., 1978, "Turbulent Airfoils for General Aviation," AIAA J. Aircraft, V15, No. 2, pp. 93-99.

4. Fergason, J. L., 1964, "Liquid Crystals," Scientific American, Vol. 211, pp. 76-85.

5. Fergason, J. L., 1968, "Liquid Crystals in Nondestructive Testing," J. Applied Optics, Vol. 7, pp. 1729-1737.

6. Klein, E. J., 1968, "Liquid Crystals in Aerodynamic Testing," Astronautics and Aeronautics, Vol. 6, pp. 70-73.

7. Klein, E. J. and Margozzi, A. P., 1969, "Exploratory Investigation on the Measurement of Skin Friction by Means of Liquid Crystals," NASA-TM-X-1774.

8. Holmes, B. J. et al., 1986, "A New Method for Laminar Boundary Layer Transition Visualization in Flight: Color Changes in Liquid Crystal Coatings," NASA-TM-87666.

9. Holmes, B. J. et al., 1986, "Advanced Transition Measurement Methods for Flight Applications," AIAA 86-9786, 3rd Flight Testing Conf., Las Vegas, Nevada.

10. Gall, P. D. and Holmes, B. J., 1986, "Liquid Crystals for High-Altitude In-Flight Boundary Layer Flow Visualization," AIAA 86-2592, General Aviation Technology Conf., Anaheim, California.

11. Reda, D. C., 1988, "Liquid Crystals for Unsteady Surface Shear Stress Visualization," AIAA 88-3841CP, Proceedings, 1st National Fluid Dynamics Congress, Cincinnati, Ohio, Part 2, pp. 1069-1072.

12. Reda, D. C., 1988, "Liquid Crystals for Surface Shear Stress Visualization on Wind Turbine Airfoils," Proceedings, WINDPOWER '88, Honolulu, Hawaii.

13. Reda, D. C. and Butterfield, C. P., 1989, "Liquid-Crystal, Shear-Stress-Visualization Experiments on a Horizontal Axis Wind Turbine," Proceedings, 8th ASME Wind Energy Symposium, Houston, Texas.

14. Anonymous, 1988, "Liquid Crystals for Windflow Visualization," mixtures TI511 and TI622, BDH Limited, Broom Rd., Poole, BH12 4NN, England (American distribution by EM Industries, Inc., Hawthorne, NY).

15. Reda, D. C. and Butterfield, C. P., 1989, "Visualization of Boundary Layer Transition Zone Movement on Oscillating Airfoils with Shear-Sensitive Liquid Crystal Coatings," Proceedings of the Symposium on Flow Visualization, ASME Winter Annual Meeting, San Francisco, California.

16. Gregorek, G. M. and Klimas, P. C., 1985, "Tailored Airfoils for Wind Turbine Applications," Proceedings, 4th ASME Wind Energy Symposium, Dallas, Texas.

17. de Vries, O., 1979, "Fluid Dynamic Aspects of Wind Energy Conversion," AGARDograph No. 243.

18. Freymuth, P., 1981, "Rotational Interference for Darrieus Rotors," ASME J. Solar Energy Engineering, Vol. 103, pp. 173-174.

19. Zaman, K. B. M. Q., McKinzie, D. J. and Rumsey, C. L., 1989, "A Natural Low-Frequency Oscillation of the Flow Over an Airfoil Near Stalling Conditions," J. Fluid Mechanics, Vol. 202, pp. 403-442.

20. Gregorek, G. M., Hoffmann, M. J. and Berchak, M. J., 1989, "Steady State and Oscillatory Aerodynamic Characteristics of a Sandia 0018/50 Airfoil," Data Report, Aeronautical and Astronautical Research Laboratory, Ohio State University.

21. Hoffmann, M. J., 1989, "Experimental Results for the SAND 0018/50 Airfoil," Proceedings 9th Vertical Axis Wind Turbine Seminar, Sandia National Laboratories, Bushland, Texas.

22. Evangelista, R., McGhee, R. J. and Walker, B. S., 1989, "Correlation of Theory to Wind-Tunnel Data at Reynolds Numbers Below 500,000," Proceedings of the Conference on Low Reynolds Number Aerodynamics (T. J. Mueller, Editor), Notre Dame University, South Bend, Indiana.

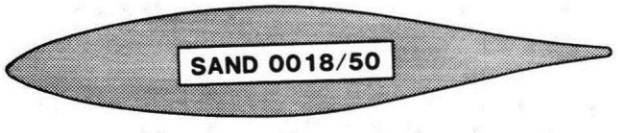

Figure 1: SAND 0018/50 Airfoil

TABLE 1: SAND 0018/50 COORDINATES

X/C	± Y/C
0	0
.003	.006
.013	.014
.027	.023
.046	.032
.070	.040
.097	.049
.129	.057
.164	.065
.201	.072
.242	.078
.285	.083
.329	.087
.375	.089
.421	.090
.468	.089
.514	.086
.561	.080
.609	.072
.657	.064
.704	.055
.751	.045
.796	.036
.838	.028
.877	.021
.912	.016
.943	.011
.967	.009
.985	.007
1.000	0.000

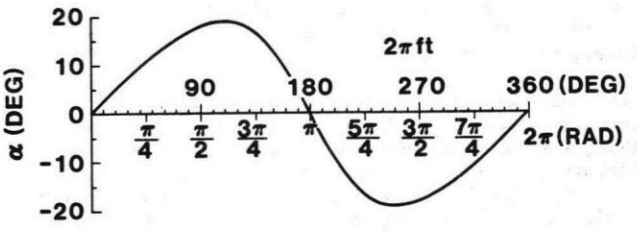

Figure 2: Angle-of-Attack Forcing Function

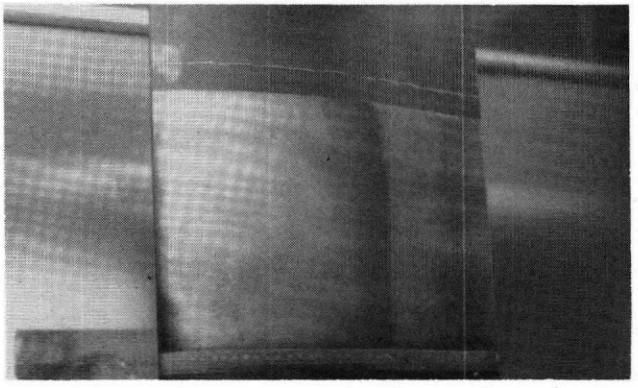

Figure 3: Black and White Photograph of Liquid Crystal Pattern, $\alpha = 0°$

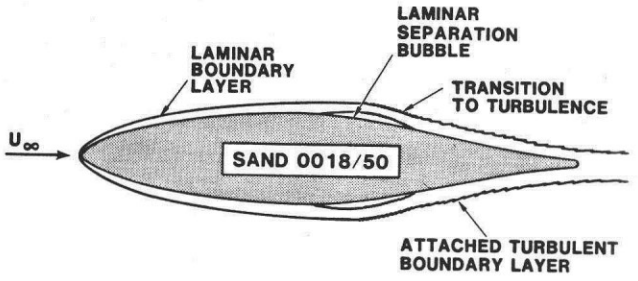

Figure 4: Flow Field Schematic, $\alpha = 0°$

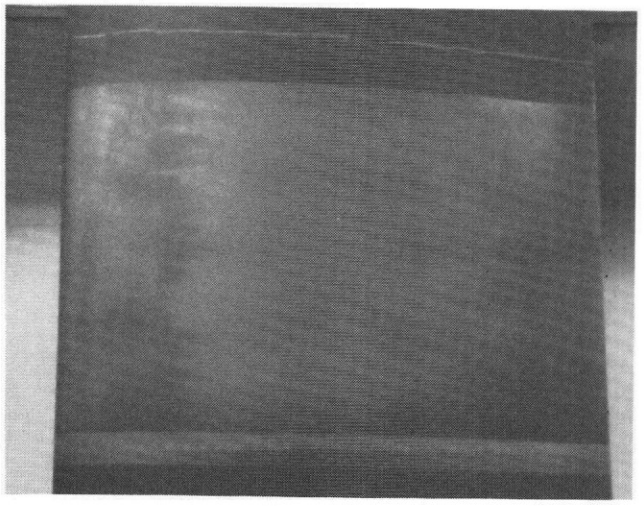

Figure 5: Black and White Photograph of Liquid Crystal Pattern, $\alpha = 6°$

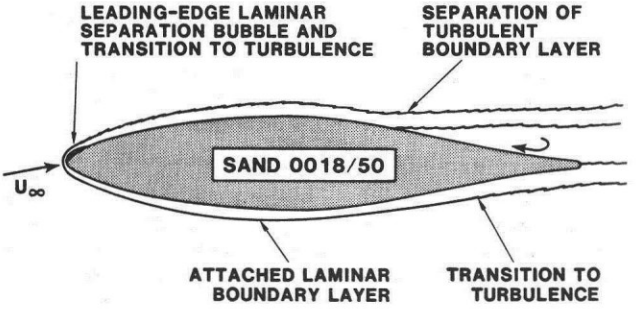

Figure 6: Flow Field Schematic, $8.5° \leq \alpha < 13.5°$

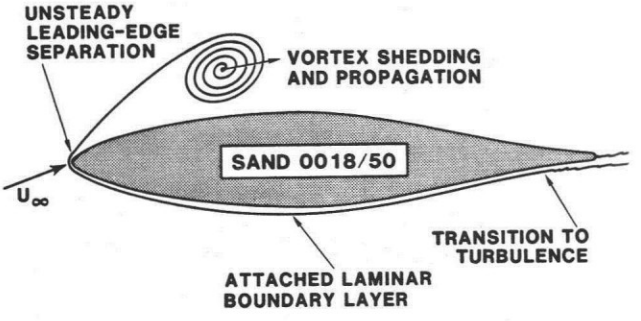

Figure 7: Flow Field Schematic, $\alpha \geq 13.5°$

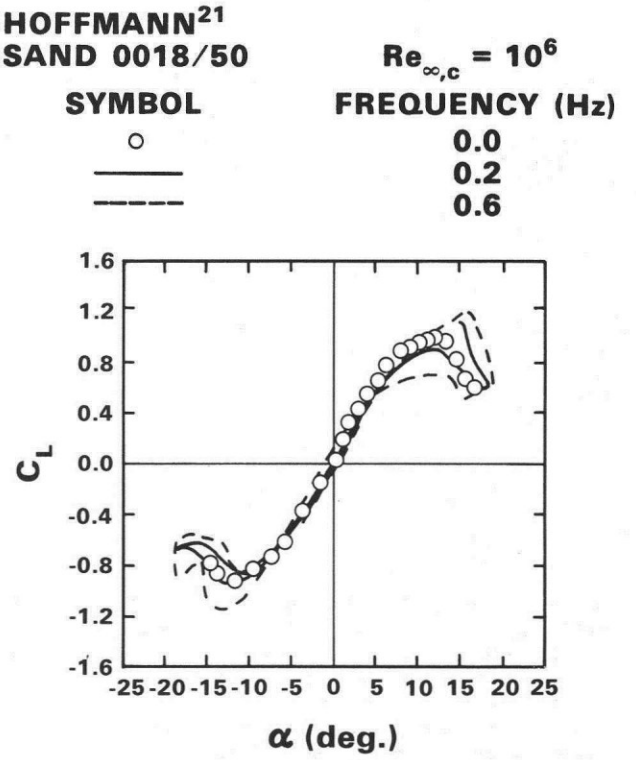

Figure 8: Lift Coefficient Versus Angle of Attack with Frequency of Oscillation as a Parameter.

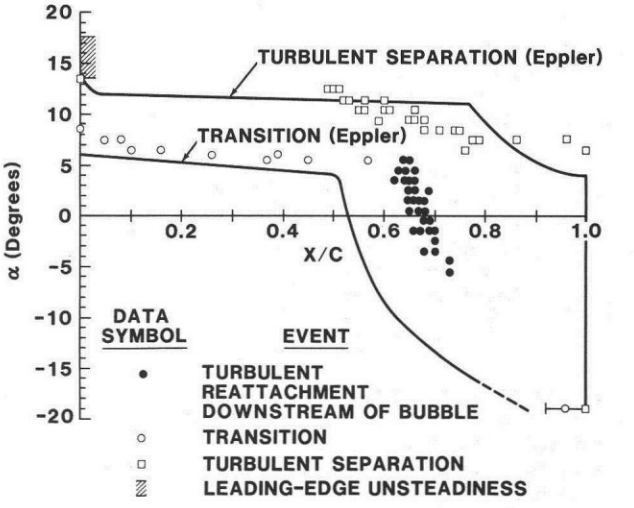

Figure 9: Transition and Turbulent Separation Locations Versus Angle of Attack; Eppler Code Predictions Compared to Measurements